ACS APPLIED MATERIALS & INTERFACES

Research Article

www.acsami.org

Assessment of the Role of Micropore Size and N-Doping in CO_2 Capture by Porous Carbons

Marta Sevilla,* Jose B. Parra, and Antonio B. Fuertes

Instituto Nacional del Carbón (CSIC), P.O. Box 73, Oviedo 33080, Spain

Supporting Information

ABSTRACT: The role of micropore size and N-doping in CO_2 capture by microporous carbons has been investigated by analyzing the CO_2 adsorption properties of two types of activated carbons with analogous textural properties: (a) N-free carbon microspheres and (b) N-doped carbon microspheres. Both materials exhibit a porosity made up exclusively of micropores ranging in size between <0.6 nm in the case of the pristine materials and up to 1.6 nm for the highly activated carbons (47% burnoff). The N-doped carbons possess ~3 wt % of N heteroatoms that are incorporated into several types of functional groups (i.e., pyrrole/pyridone, pyridine, quaternary, and pyridine-*N*-oxide). Under conventional operation conditions (i.e., $T \sim 0-25$ °C and $P_{CO2} \sim 0-1$ bar), CO_2 adsorption proceeds via a volume-filling mechanism, the size limit for volume-filling being ~0.7−0.8 nm. Under these circumstances, the adsorption of CO_2 by nonfunctionalized porous carbons is mainly determined by the volume of the micropores with a size below 0.8 nm. It was also observed that the CO_2 capture capacities of undoped and N-doped carbons are analogous which shows that the nitrogen functionalities present in these N-doped samples do not influence CO_2 adsorption. Taking into account the temperature invariance of the characteristic curve postulated by the Dubinin theory, we show that CO_2 uptakes can be accurately predicted by using the adsorption data measured at just one temperature.

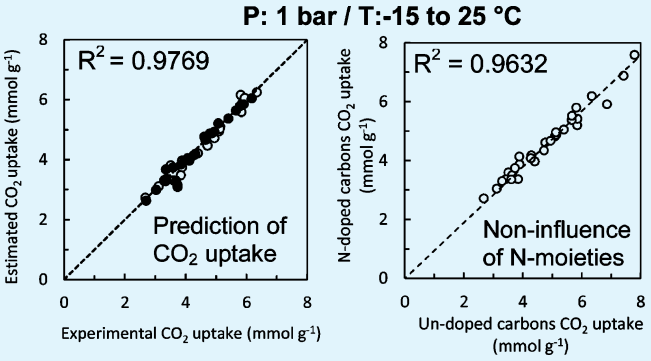

KEYWORDS: *adsorption, porosity, N-doping, CO_2 capture, carbon*

INTRODUCTION

CO_2 capture by means of adsorption in porous materials using pressure and/or temperature swing approaches is receiving increasing attention due to the advantages it offers over conventional technologies based on aqueous amine solvents. These advantages include reduced energy consumption for regeneration, greater capture capacity, ease of handling, reduced environmental impact, etc. A great deal of research effort is therefore being directed toward the design and synthesis of high performance porous sorbents for CO_2 capture from flue gas. Such sorbents are superior in terms of capacity, stability, kinetics, selectivity, and regeneration. A wide range of sorbents has been analyzed, including porous carbons,[1−3] zeolites,[4,5] MOFs,[6,7] and microporous polymers.[8,9] Especially, high CO_2 adsorption capacities have been achieved with microporous carbon materials.[2,10] Recently, Presser et al. empirically deduced that, in the case of microporous carbons, CO_2 capture at atmospheric pressure is very much dependent on the number of micropores smaller than 0.8 nm.[1] Following their initiative, Wei et al. and Sevilla et al. found similar results for a variety of activated carbons.[11,12] However, neither of them provides any explanation as to why micropores of this size are important for the adsorption of CO_2 molecules.

Some authors have tried to enhance the interaction of porous carbons with CO_2 molecules by mimicking the amine scrubbing process (i.e., by grafting/impregnating amines or by introducing basic nitrogen functionalities into the porous framework). This last method can be tackled either by (i) carbonizing the N-containing precursor or mixtures of nitrogen-containing organic compounds (i.e., melamine, urea, etc.) with N-free materials[13−15] or by (ii) heat-treatment with N-containing gases (i.e., NH_3).[16,17] Amine-functionalization has been proved to lead to an enhancement of the isosteric heat of adsorption (40−90 kJ/mol),[18−20] yielding values typical of a chemisorption process, which makes it possible to adsorb at higher temperatures and improve selectivity. However, this is achieved at the expense of a drastic drop of the porous properties.[21] This has directed the attention of researchers to the study of N-doping of carbon materials as an alternative method of increasing CO_2 capture capacity. Indeed, several authors have suggested that the presence of N heteroatoms in carbonized-activated carbons enhances their performance for CO_2 capture.[3,14,22−26] However, to attribute this enhancement solely to N functionalities is impossible due to the fact that other factors, such as micropore size distribution or micropore volume, also play an important role. In fact, most of the works in this area analyze exclusively

Received: April 18, 2013
Accepted: June 10, 2013
Published: June 24, 2013

   dx.doi.org/10.1021/am401423b | ACS Appl. Mater. Interfaces 2013, 5, 6360−6368

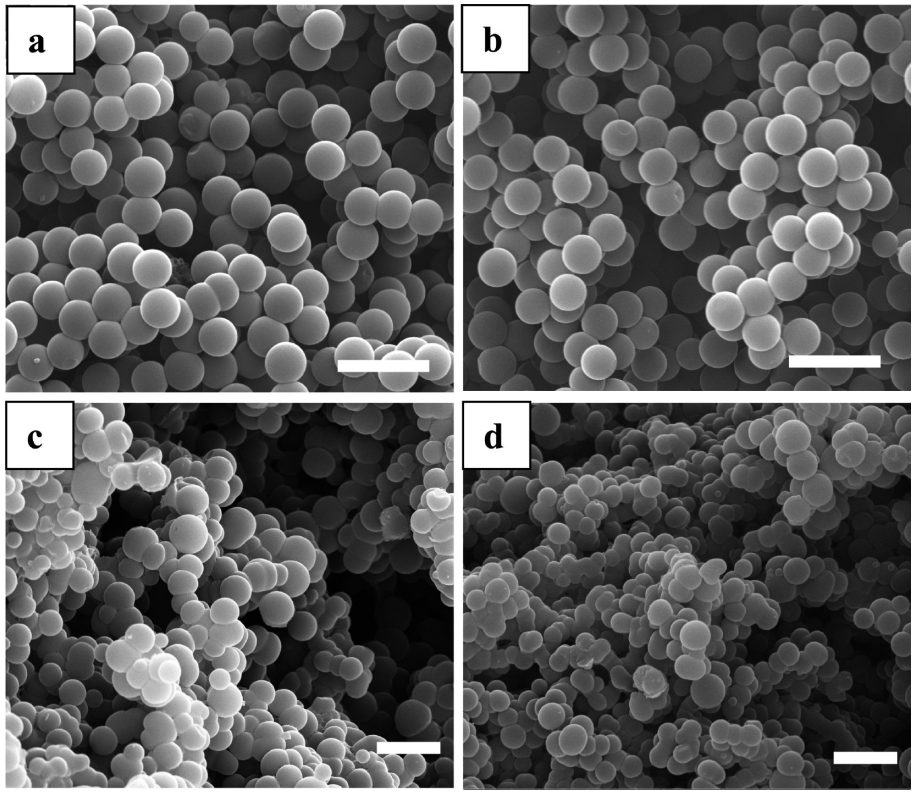

Figure 1. SEM images of Stöber-based carbon microspheres (a, b) and N-doped carbon spherules (c, d) of nonactivated (a, c) and activated samples at 35% burnoff (b, d). Bar scale = 2 μm.

the performance of N-doped carbons without any reference to undoped carbons with similar textural properties. Furthermore, the benefits attributed to N-doped carbons with respect to undoped carbons in relation to CO_2 capture are in many cases merely marginal. Therefore, up to date, there is no clear evidence about the role that N heteroatoms present in carbonized-activated materials play in CO_2 adsorption.

Bearing in mind these ideas, the main objectives of this study are: (a) to clarify the effect that the size of the micropores has on CO_2 adsorption capacity and (b) to evaluate the importance of the presence of N heteroatoms for CO_2 capture. In order to attain these objectives, we decided to appraise each of these contributions separately by using microporous carbons with similar textural properties but differing in their N-content. To this end, we prepared two activated carbon series: (a) five samples with activation degrees in the 0−47% range and (b) five samples with similar burnoff degrees but containing around 3 wt % nitrogen. Special care was taken to ensure that, for each activation degree, the undoped and N-doped samples had similar textural properties. In order to determine the role of micropore size, special attention was paid to the fabrication of materials with uniform micropores. The synthesis of such materials was carried out by physical activation with CO_2 as activating agent. To ensure uniform micropore development, the gasification reaction was carried out close to chemical control and diffusional restrictions were minimized. To meet this requirement, we used small porous carbonaceous particles (<1 μm) as starting material and the reaction with CO_2 was carried out at very slow gasification rates ($\sim$ 1−2%·h^{-1}).

RESULTS AND DISCUSSION

Structural and Textural Properties of Porous Carbons.

The (resorcinol-formaldehyde)-based carbon consists of uniform colloidal spheres that have a smooth surface and a mean diameter of 0.82 ($\pm$0.06) μm (Figure 1a), whereas the N-doped carbon is formed by interconnected microspheres with a diameter of around 1 μm (Figure 1c). In both cases, after activation, the surface of the particles remains smooth and no roughness is observed. Furthermore, the diameter of the carbon microspheres hardly changes throughout the gasification process, as can be seen from the SEM images of nonactivated (Figure 1a,c) and activated carbons (burnoff: 35%) (Figure 1b,d). This is corroborated by the size distribution histograms shown in Figure S1 (Supporting Information) for the C-0 and C-3 samples. These results reveal that the mass loss produced as a consequence of the gasification process occurs mainly in the bulk of the carbon particles instead of the surface, which suggests that the gasification reaction proceeds uniformly throughout the carbon particles.

The textural properties of the different porous carbons were analyzed by means of gas adsorption of nitrogen at −196 °C and CO_2 at 0 °C. Figure 2a,b compares the nitrogen sorption isotherms for the two series of samples. It can be seen that all the samples exhibit a type I isotherm, which is typical of microporous materials. Moreover, these isotherms exhibit two important characteristics: (a) narrow knees at a low relative pressure (p/p_o < 0.03) and (b) an absence of adsorption in the pressure range of 0.03−0.9. These results show that the porous carbons have a narrow micropore size distribution and that no mesoporosity is generated during the activation process regardless of the activation degree. In addition, as the activation proceeds, a slight widening of the knee of the isotherms takes

dx.doi.org/10.1021/am401423b | ACS Appl. Mater. Interfaces 2013, 5, 6360−6368

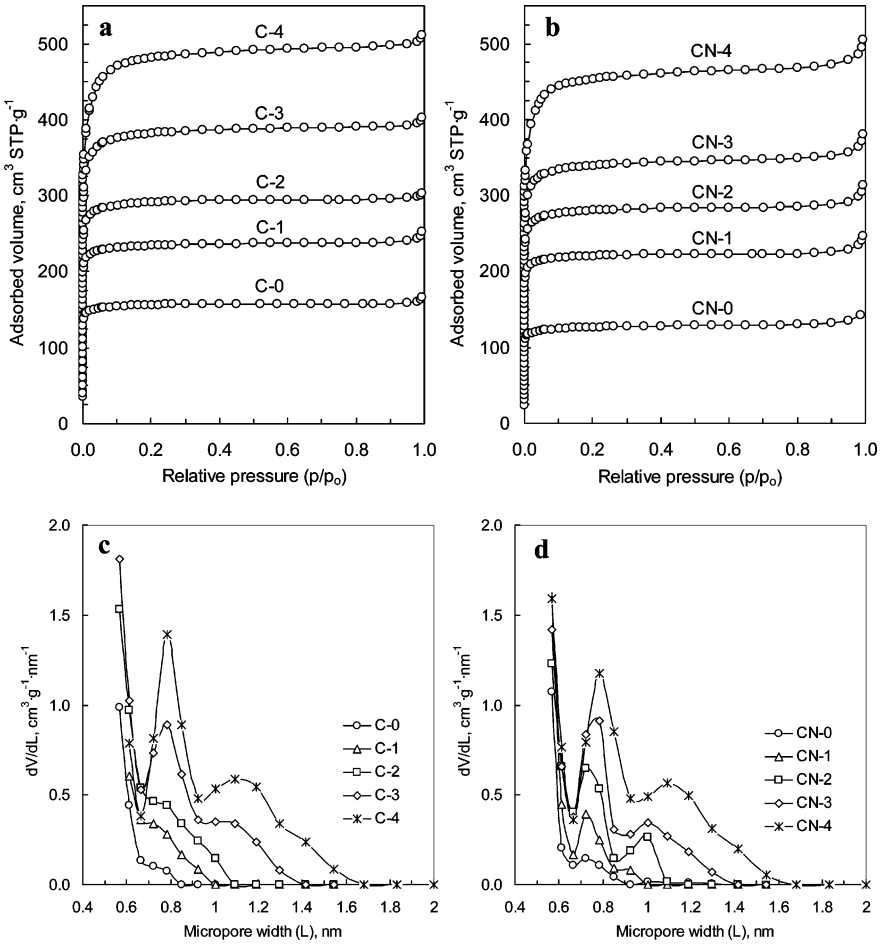

Figure 2. Nitrogen sorption isotherms (a, b) and micropore size distributions (c, d) of activated samples.

Table 1. Textural Parameters Deduced from the N_2 (−196 °C) and CO_2 (0 °C) Adsorption Data

			N_2 adsorption at −196 °C				CO_2 adsorption at 0 °C (D−R)				
								micropore system I		micropore system II	
sample code	N (wt %)	burn-off (%)	S_{BET} ($m^2 \cdot g^{-1}$)	S^t_m ($m^2 \cdot g^{-1}$)	V_p ($cm^3 \cdot g^{-1}$)	V^t_m ($cm^3 \cdot g^{-1}$)	V_o (c $m^3 \cdot g^{-1}$)	$V_{o\,I}$ ($cm^3 \cdot g^{-1}$)	L_I(nm)	$V_{o\,II}$ ($cm^3 \cdot g^{-1}$)	L_{II}(nm)
C-0		0	640	630	0.26	0.24	0.30			0.30	0.55
C-2		24	1180	1170	0.47	0.45	0.44	0.12	0.47	0.32	0.63
C-3		35	1530	1520	0.62	0.59	0.52	0.22	0.57	0.30	0.74
C-4		47	1920	1900	0.79	0.74	0.56	0.20	0.58	0.36	0.81
CN-0	3.19	0	510	500	0.22	0.20	0.26			0.26	0.51
CN-1	2.73	15	900	890	0.38	0.34	0.35			0.35	0.56
CN-2	2.53	24	1160	1130	0.48	0.43	0.39	0.08	0.42	0.31	0.61
CN-3	3.16	35	1360	1340	0.59	0.52	0.43	0.15	0.50	0.28	0.65
CN-4	3.13	47	1810	1790	0.78	0.70	0.48	0.04	0.38	0.44	0.72

place, which suggests an increase in micropore size. This is confirmed by the micropore size distributions (MPSDs) obtained by means of the QSDFT method (Figure 2c,d). These clearly show that a gradual widening of the MPSDs occurs as the activation degree increases. The porosity of the nonactivated samples (i.e., C-0 and CN-0) is made up almost exclusively of very narrow micropores (<0.6 nm). As the activation progresses, an enlargement of micropores takes place and, in the case of the medium-activated samples (i.e., C-1, C-2, CN-1, and CN-2), a significant fraction of the micropores has sizes in the 0.6−1.1 nm range. This is especially evident in the case of the CN samples which exhibit a well-defined maximum of MPSD at 0.7−0.8 nm. Three well-defined micropore ranges can be distinguished for the highly activated samples (i.e., C-3, C-4, CN-3, and CN-4): (I) very narrow micropores (size <0.6 nm), (II) micropores with sizes in the 0.7−0.9 nm range (maximum at ∼0.8 nm), and (III) supermicropores with sizes in the 0.9−1.6 nm range (maximum at ∼1.1 nm), which appear exclusively at high activation degrees.

The textural properties obtained from the analysis of the nitrogen isotherms are shown in Table 1: (a) apparent surface area (S_{BET}), (b) total pore volume (V_p), (c) micropore surface area (S^t_m), and micropore volume (V^t_m) deduced by means of the t-plot method. Table 1 also shows the textural properties

dx.doi.org/10.1021/am401423b | ACS Appl. Mater. Interfaces 2013, 5, 6360−6368

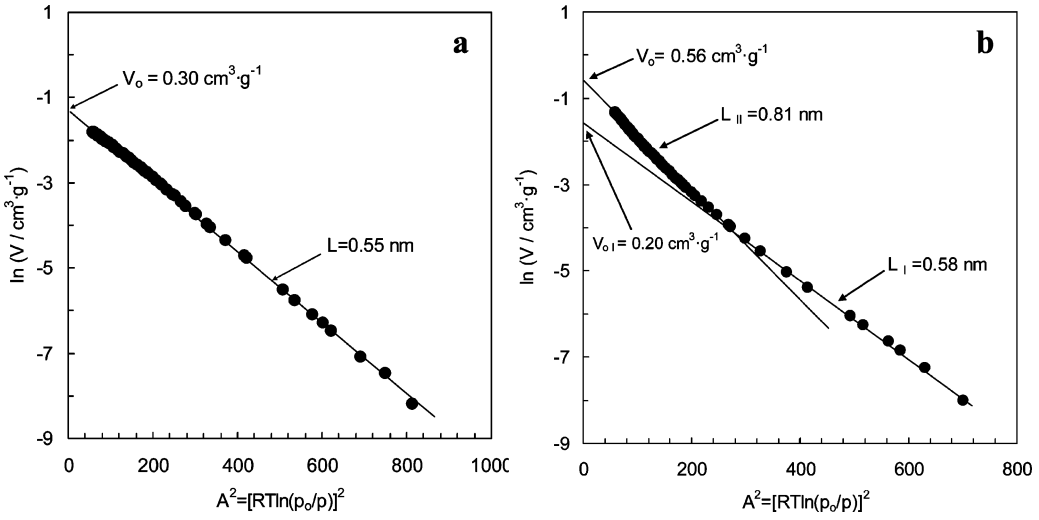

Figure 3. D−R plots for the adsorption of CO_2 by (a) C-0 and (b) C-4 samples at 0 °C.

corresponding to the narrow micropores (i.e., micropore volume and average micropore size), which were deduced by applying the Dubinin−Radushkevich (D−R) equation to the CO_2 adsorption data at 0 °C. The apparent surface areas (S_{BET}) regularly increase with the degree of burnoff from 637 $m^2·g^{-1}$ (C-0) or 510 $m^2·g^{-1}$ (CN-0) to 1920 $m^2·g^{-1}$ (C-4) or 1810 $m^2·g^{-1}$ (CN-4), respectively. They are similar to the microporous surface areas (S_m^t) deduced from the t-plot method, which suggests that the porosity of these samples is formed exclusively by micropores. This is confirmed by the fact that the total pore volumes (V_p) are quite close to the micropore volume obtained by the t-plot method (V_m^t). A comparison of the micropore volumes deduced from the N_2 (t-plot, V_m^t) and CO_2 (D−R plot, V_o) adsorption data reveals two interesting features. In the case of the nonactivated samples, $V_o > V_m^t$, reflecting the restriction of the diffusion of N_2 molecules in the narrow micropores (<0.6 nm) (see Figure 2c,d). This is a consequence of the low temperature employed in these experiments. In contrast, for the highly activated carbons (i.e., 35% and 47% burn-offs) with micropore sizes of up to 1.6 nm (see Figure 2c,d), $V_o < V_m^t$, which is due to the fact that CO_2 adsorption is restricted to micropores below 0.8 nm (vide infra).

The CO_2 D−R plots provide interesting information about the size of the narrow micropores (<0.8 nm). Indeed, the slope calculated from the linear form of the D−R equation can be used to estimate the average size of the narrow micropores (L), as mentioned in the Experimental Section. In the case of the nonactivated samples, the D−R plot shows a well-defined linear behavior over the entire A^2 range (see Figure 3a). This result shows that the porosity of these samples is made up of uniform micropores, with a size of around 0.5 nm, as deduced from eq 2. It is worth noting that this micropore size is similar to that obtained by the QSDFT method (see Figure 2c,d). In contrast, the D−R plots corresponding to the activated samples are nonlinear and they exhibit upward deviations at high A^2 values, i.e., at low relative pressures (see Figure 3b). These deviations appear to be due to the fact that the narrow microporosity is made up of micropores of various sizes. In cases like this, Dubinin et al. postulated the existence of two micropore systems.[27] In this study, we adopted this approach and applied it to the CO_2 adsorption data of the activated samples, as illustrated in Figure 3b for the C-4 sample. The values of the micropore volume and micropore size corresponding to both pore systems are listed in Table 1. It can be observed that the pore system corresponding to the narrowest pores (System I) is made up of micropores with average widths of around 0.5 nm and that this size hardly changes with the degree of activation. On the other hand, as the activation progresses, a widening of a certain number of micropores (System II) takes place, whose size gradually increases up to ∼0.7−0.8 nm in the case of the samples with 47% burnoff. Again, these results agree with those deduced by the QSDFT method. In fact, micropore systems I and II deduced from the D−R analysis correlate very well with the ranges I and II identified in the MPSDs shown in Figure 2c,d. On the other hand, micropore range III (supermicropores with sizes of ∼0.9−1.6 nm), which also appears in these figures, cannot be detected by means of D−R analysis of the CO_2 isotherms because, under these conditions (0 °C, 1 bar), the adsorption of this gas is limited to micropores below 0.8 nm (vide infra).

Relevance of Micropore Size for CO_2 Adsorption. For nonpolar adsorbate molecules and nonfunctionalized adsorbent surfaces, the adsorbate−adsorbent interaction energy is derived from short-range attractive and repulsive forces (nonspecific interactions).[28] This interaction energy is substantially enhanced when the adsorption takes place in very narrow pores because of the overlapping of the potential fields from the neighboring walls.[29] This enhanced adsorption potential can lead to the complete filling of the narrow micropores at very low relative pressures (p/p_o < 0.01). Under these circumstances, the adsorption mechanism consists of volume-filling rather than surface coverage typical of meso-macroporous materials and the adsorbate molecules occupying these narrow micropores are in a liquid-like state.[30] A description of the volume-filling mechanism has been provided by Dubinin, who deduced a relationship between the degree of micropore-filling and the partial pressure of the adsorbate (D−R equation).[31] Theoretical calculations have demonstrated that enhancement of the adsorption energy is negligible for micropore widths larger than around two times (slit-shaped pores) or three times (cylindrical-shaped pores) the molecular diameter.[32] Taking into account that the shape of micropore in carbonaceous materials is closer to a slit than a cylinder, the size limit for volume-filling can be established at ∼0.7−0.8 nm for CO_2 (Kinetic diameter of CO_2 ∼ 0.33 nm). This result is very

important in relation to CO_2 capture by carbonaceous adsorbents under conventional operational conditions (temperatures in the 0−25 °C range and CO_2 pressures in the 0−1 bar range). In fact, under these circumstances, the CO_2 relative pressures are very low ($p/p_o < 0.03$) and the adsorption of CO_2 occurs via a volume-filling mechanism. Thus, it can be inferred that, at these low relative pressures, only those adsorbents with a large number of narrow micropores below ~0.8 nm will be able to capture appreciable amounts of CO_2. This result clearly suggests that the amount of CO_2 captured by nonfunctionalized porous carbons is mainly determined by the volume of micropores with a size below 0.8 nm. This conclusion is similar to that which was empirically deduced by Presser et al. by correlating the CO_2 uptakes and the micropore volumes of a variety of CDCs.[1] Conversely, other pores present in porous carbons, such as supermicropores (0.8−2 nm) or mesopores (>2 nm), are not relevant for CO_2 capture under conventional operational conditions (i.e., $T \sim 0$−25 °C, $p_{CO2} \leq 1$ bar). This is because they are unable to adsorb significant CO_2 amounts at the very low relative pressures existing under such conditions. This is the reason for the lack of correlation between the CO_2 adsorption capacity of porous carbons and their overall textural properties such as total pore volume or BET surface area. At this point, it is important to mention that, when the adsorption is performed up to pressures close to saturation (i.e., 35 or 64 bar at 0 or 25 °C, respectively), the adsorption of CO_2 will occur like that of N_2 (−196 °C) in comparable relative pressure ranges.[33] Under these circumstances, CO_2 uptakes can be notably enhanced because supermicropores are now able to adsorb CO_2 via the coverage adsorption mechanism.

Comparison of the shape of the CO_2 isotherms corresponding to the pristine materials and activated carbons clearly evidence the enhanced adsorption potential in the materials with the narrowest pores. This is illustrated in Figure 4, where

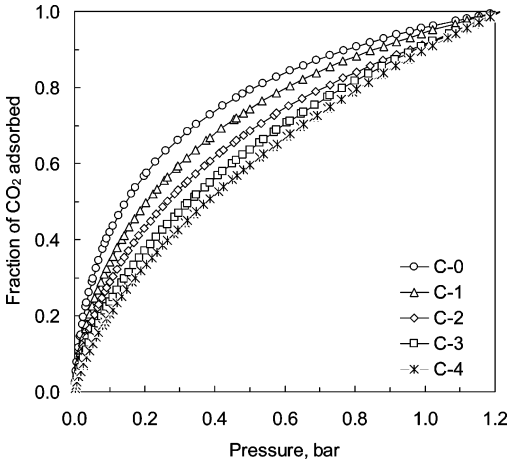

Figure 4. Comparison of the fraction of CO_2 adsorbed by undoped carbons at different activation degrees. Adsorption temperature of 0 °C.

the CO_2 adsorbed at different burn-offs is compared at an adsorption temperature of 0 °C. It can be seen that the fraction of CO_2 adsorbed at a given pressure decreases with activation degree. This result clearly suggests a reduction in the adsorption potential as a result of the enlargement of the micropores as the activation progresses. Similar results have been obtained for other adsorption temperatures (see Figure S2 in the Supporting Information).

An insight into the role of micropores in CO_2 adsorption can be obtained by analyzing the relationship between the micropore size and the fraction of micropore volume filled by CO_2 (f_{CO2}). This parameter is defined as $f_{CO2} = q/(V_m \cdot \rho_{CO2})$, where q is the CO_2 uptake, V_m is the micropore volume (V_o or V_m^t), and ρ_{CO2} is the density of liquid CO_2 (1.03 g·cm^{-3} at 0 °C). When the f_{CO2} parameter corresponding to micropores <0.8 nm (micropore volume = V_o) is represented vs the average micropore width L_{II} (Figure 5a), it can be seen that, for average

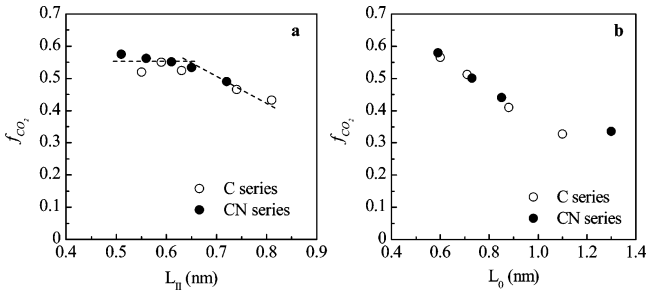

Figure 5. Modification of f_{CO2} parameter with average micropore size deduced by applying the D−R plot to the (a) CO_2 adsorption (0 °C) and (b) N_2 adsorption (−196 °C) isotherms.

micropore widths <0.65−0.7 nm, f_{CO2} remains almost constant, whereas for average micropore widths in the ~0.7−0.8 nm range, there is a slight decrease in f_{CO2}. This result shows that, even for average micropore widths of ~0.7−0.8 nm, there is already a decrease in the enhancement of the adsorption potential. This decrease is even more pronounced if f_{CO2} is determined taking into account the complete range of micropores (micropore volume = V_m^t). Thus, as shown in Figure 5b, f_{CO2} steadily decreases with the increase in the average micropore width (L_o) deduced by applying the D−R equation to the N_2 sorption isotherm. This result is in agreement with the fact that it is micropores below 0.8 nm that are mainly responsible for CO_2 adsorption at the low relative pressures used in the experiments carried out under conventional conditions.

The variation in CO_2 adsorption with temperature might help to clarify the importance of micropore size in this process. In Figure 6a, the modification of CO_2 uptakes (measured at 1 bar) with the degree of activation is represented at three temperatures for both series. It can be seen that, whereas at 25 °C the CO_2 uptakes hardly change with burnoff, at −15 °C a

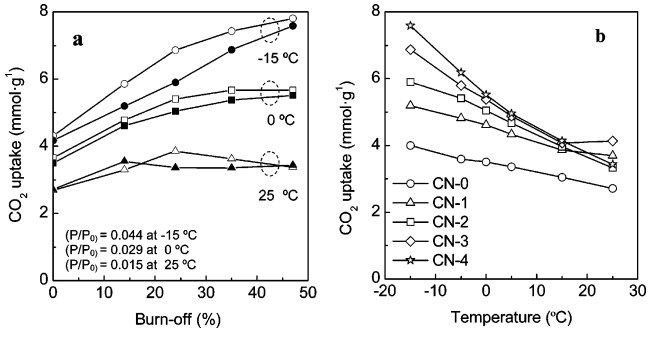

Figure 6. Modification of CO_2 uptake (p_{CO2} = 1 bar) with (a) burnoff for undoped (open symbols) and N-doped (black symbols) samples and (b) adsorption temperature for N-doped carbons with different activation degrees.

dx.doi.org/10.1021/am401423b | ACS Appl. Mater. Interfaces 2013, 5, 6360−6368

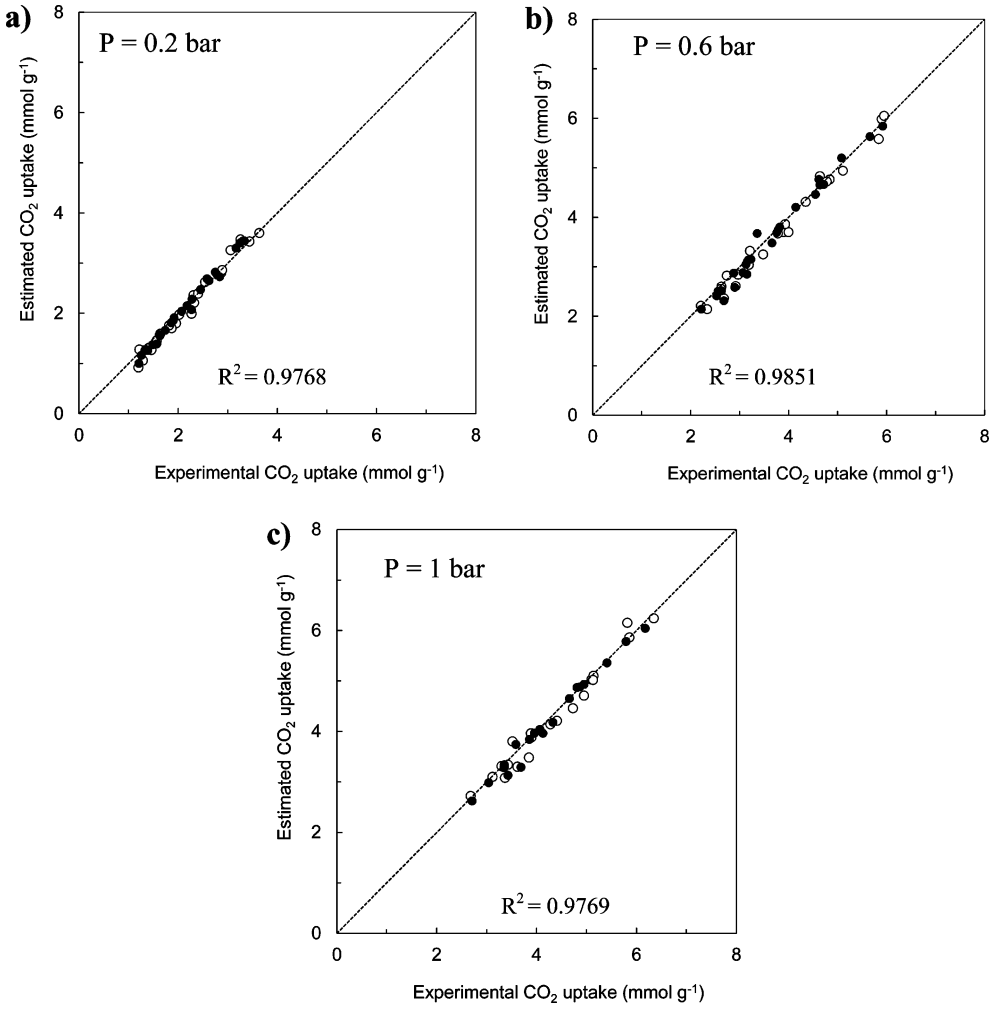

Figure 7. Correlation between the experimental CO_2 uptakes and those estimated from CO_2 adsorption data measured at 0 °C: (a) 0.2 bar, (b) 0.6 bar, and (c) 1 bar. Open symbols refer to undoped samples and black symbols to N-doped carbons.

notable increase occurs. This is due to the fact that at 25 °C only the narrowest micropores are able to adsorb CO_2 because of the low relative pressures ($p/p_o \sim 0.015$ at 25 °C for p_{CO2} = 1 bar). In contrast, at lower adsorption temperatures such as −15 °C, the CO_2 uptake increases substantially with burnoff. This is a consequence of the fact that a certain number of micropores >0.8 nm are now able to adsorb CO_2 owing to the higher relative pressures involved ($p/p_o \sim 0.044$ at −15 °C for p_{CO2} = 1 bar). At this point, it is important to examine the effect of adsorption temperature upon CO_2 uptake (p = 1 bar). Because adsorption is an exothermic process, in general, CO_2 uptake diminishes with temperature. However, the effect of temperature on the quantity of CO_2 adsorbed also depends on the pore structure of the adsorbent (i.e., pore size distribution). This is evidenced by the results shown in Figure 6b, where the variation in CO_2 uptake with temperature is represented for several CN samples by different activation degrees. Interestingly, whereas for the nonactivated CN-0 sample (micropores <0.6 nm), the CO_2 uptake diminishes only slightly with temperature, for the highly activated CN-4 sample (micropores up to 1.6 nm), a significant drop is observed. This finding is in accordance with the above results and confirms that the use of subzero adsorption temperatures can substantially enhance the CO_2 uptakes of highly activated carbons with wide micropore size distributions.

Prediction of CO_2 Adsorption Uptakes in Activated Carbons. It will now be shown that, by applying Dubinin's concepts to CO_2 adsorption in carbonaceous materials, it is possible to estimate the amounts of CO_2 adsorbed at different temperatures by using the adsorption data measured at only one temperature. Indeed, the fundamental postulate of the potential theory is the assumption that the adsorption potential is independent of the temperature and that it exclusively depends on the characteristics of the adsorbent−adsorbate system.[34] This essentially means that, for a given sample, the characteristic curves (i.e., V vs $RT \ln(p_o/p)$) should be temperature invariant. The characteristic curves for the C-2 and CN-2 samples at five adsorption temperatures are shown in Figure S3 in the Supporting Information. These curves satisfactorily fulfill the temperature invariance condition. From this, it can be inferred that, by measuring CO_2 adsorption at a single temperature (usually at 0 °C) and calculating the characteristic curve, inverse calculations can be made to obtain isotherms at any other temperature over a range below the critical temperature. In other words, for a particular sample, the CO_2 adsorption data (isotherm) measured at a given temperature will allow the prediction of CO_2 uptakes at other temperatures. Figure 7 shows a comparison between the experimental and calculated CO_2 uptakes at several temperatures (−15, −5, +5, +15, and +25 °C) and pressures of 0.2 bar

dx.doi.org/10.1021/am401423b | ACS Appl. Mater. Interfaces 2013, 5, 6360−6368

(Figure 7a), 0.6 bar (Figure 7b), and 1 bar (Figure 7c). The CO_2 adsorption data measured at 0 °C for the $C-x$ and $CN-x$ samples were used as reference. It can be seen that there is an excellent agreement between both sets of data. This result shows that the CO_2 uptakes at several temperatures can be accurately predicted by using the adsorption data experimentally measured at a given temperature.

Influence of Nitrogen on CO_2 Capture. As mentioned in the Introduction section, our strategy for elucidating the role of N heteroatoms in CO_2 capture is based on the comparison of the CO_2 performance of undoped and N-doped activated carbons with similar textural properties. The textural data listed in Table 1 reveal that the properties of $C-x$ and $CN-x$ samples are very similar. It follows that, since undoped and N-doped samples only differ in their N content, a comparison of their CO_2 performances will provide information about the role that nitrogen functionalities in the carbonized-activated materials play in CO_2 adsorption.

Independently of the activation degree, the $CN-x$ samples contain around 3 wt % nitrogen (see Table 1). The nature of the nitrogen functionalities present in the $CN-x$ samples was investigated by means of X-ray photoelectron spectroscopy (XPS). Figure S4a (Supporting Information) illustrates the different kinds of N moieties identified in the analysis of the N 1s core level XPS spectra corresponding to the CN-0 and CN-4 samples (Figure S4b in the Supporting Information). The following N functional groups were identified: (a) pyridinic-N (N-6) at 398.3 eV, (b) pyrrole/pyridone (N-5) at 400−400.4 eV, (c) quaternary-N (N-Q) at 401.2 eV, and (d) pyridine-N-oxide (N-X) at 402.8 eV. Quantitative analysis reveals that the nitrogen in nonactivated and activated samples preferentially forms N-6 (~ 40 at. %) and N-Q (24 - 34 at. %) groups, in the order N-6 > N-Q > N-5 > N-X (see Table S1 in the Supporting Information).

To analyze the effect of nitrogen upon CO_2 performance, we should envisage two scenarios. In the first scenario, the nitrogen heteroatoms present in the carbonized-activated samples are inactive toward CO_2 adsorption. Under these circumstances, the amount of CO_2 adsorbed will depend exclusively on the adsorption temperature and textural properties. The second scenario involves the assumption that the N groups have a positive effect on CO_2 adsorption and that in consequence a better CO_2 performance can be expected for the N-doped than for the undoped samples with similar textural properties. To elucidate the more probable scenario, we compared the CO_2 uptakes measured at a given temperature (p_{CO2} = 1 bar) for undoped and N-doped carbons with analogous textural properties (i.e., similar activation degrees). The comparison of both sets of data is provided in Figure 8. The results reveal that most of the represented points are below the diagonal line, which suggests that the nitrogen in the N-doped samples does not enhance CO_2 performance with respect to the undoped carbons. What is more, the correlation between these data (dotted line in Figure 8) reveals that the CO_2 uptakes in the case of the undoped samples are a little better, which is probably because of their slightly better textural properties (see Table 1). On the other hand, Figure 9 compares the adsorption isotherms of C-0/CN-0 (Figure 9a) and C-4/CN-4 (Figure 9b) at three representative temperatures (−15, 0, and 25 °C). Remarkably, no significant differences can be appreciated between the isotherms of the undoped and N-doped samples over the whole pressure range. These results lend strong support to the view that N heteroatoms present in the carbon framework of carbonized-activated carbons do not improve the uptake of CO_2. Naturally, this conclusion refers exclusively to carbons with nitrogen functionalities similar to those of the CN samples reported here (i.e., N-5, N-6, N-Q, and N-X groups). On the other hand, the possibility that the presence of other N-groups (i.e., pendant amine groups) enhances the CO_2 adsorption capacity of porous carbons cannot be excluded.

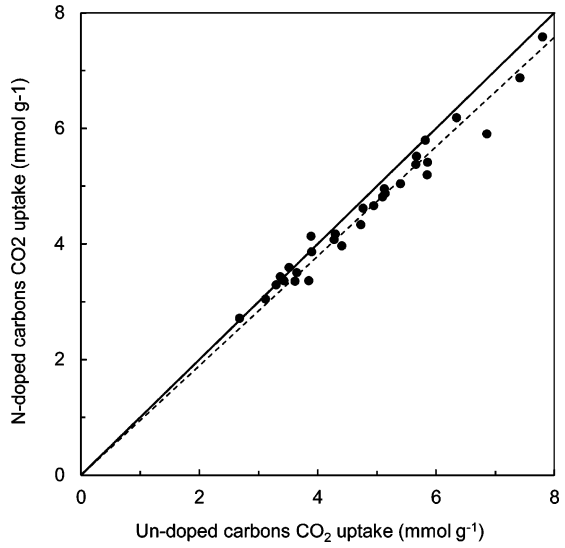

Figure 8. Comparison of CO_2 uptakes (p_{CO2} = 1 bar) of undoped (x-axis) and N-doped (y-axis) samples. The dashed line shows the fitting of the experimental data ($y = 0.95x$, $R^2 = 0.9632$).

CONCLUSIONS

N-Free and N-doped microporous carbons with analogous textural properties and tunable micropore sizes have been successfully prepared by the physical activation of (resorcinol−formaldehyde)-based carbon microspheres and a N-doped polymeric carbon produced from poly(benzoxazine-*co*-resol), respectively. Both sets of materials exhibit uniform pore size distributions in the micropore range, this porosity being composed exclusively of narrow micropores (<0.6 nm) in the case of the pristine materials and micropores of up to 1.6 nm in that of the highly activated samples. The N-doped carbons contain ~3 wt % of nitrogen which is incorporated in different functional groups such as pyridinic-N, quaternary-N, pyrrolic-/pyridonic-N, and pyridine-N-oxide. The unique textural and chemical properties of these carbon series are the key to evaluating the role of micropore size and N-doping in CO_2 adsorption. What is beyond doubt is that CO_2 adsorption by microporous carbons depends heavily on micropore size. Thus, under conventional operation conditions (T = 0−25 °C and p_{CO2} = 0−1 bar), CO_2 adsorption in porous carbons takes place via a volume-filling mechanism and the micropore size limits for volume-filling are ~0.7−0.8 nm. Therefore, CO_2 adsorption by nonfunctionalized porous carbons is mainly determined by the volume of micropores with sizes below 0.8 nm. At subzero temperatures, supermicropores also contribute to CO_2 adsorption because of the increase in relative pressure at these temperatures (i.e., $p/p_o \sim 0.044$ at −15 °C for p_{CO2} = 1 bar). It follows, therefore, that in the case of highly activated carbons with wide micropore size distributions, CO_2 performance can be considerably enhanced by carrying out the adsorption process at subzero temperatures. It has also been shown that the nitrogen functionalities present in the

dx.doi.org/10.1021/am401423b | ACS Appl. Mater. Interfaces 2013, 5, 6360−6368

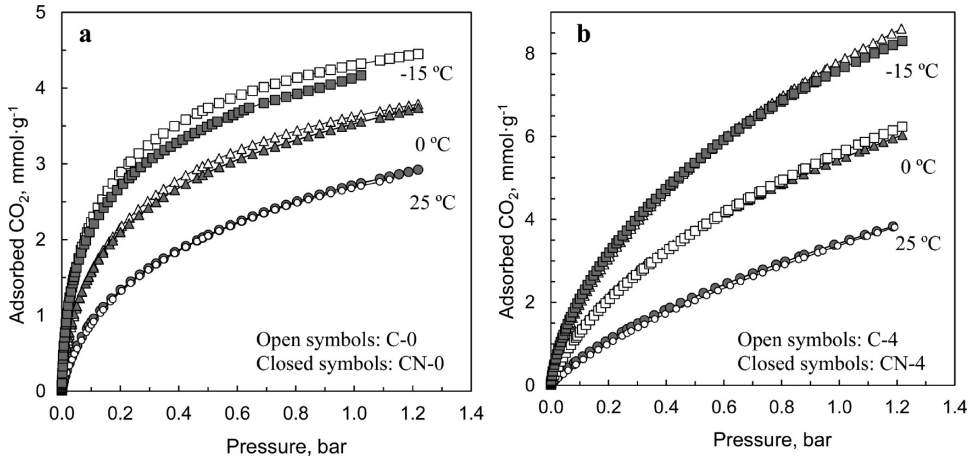

Figure 9. Comparison of CO_2 isotherms at several temperatures for (a) nonactivated and (b) activated carbons at a burnoff of 47%.

microporous carbons analyzed in this study do not have any appreciable influence on CO_2 adsorption. Finally, we demonstrated that, by taking into account the temperature invariance of the characteristic curve postulated by the Dubinin theory, CO_2 uptakes can be accurately predicted on the basis of the adsorption data obtained at just one temperature.

EXPERIMENTAL SECTION

Synthesis of Porous Carbons. *Stöber Carbon Microspheres.* Resorcinol–formaldehyde microspheres were synthesized according to the procedure reported by Liu et al.[35] Briefly, 1.05 g of ammonia aqueous solution (5 M) was added to 94 g of an ethanol–water mixture (ethanol/water volume ratio = 0.4) and stirred at 30 °C for 10 min. Afterward, 0.71 g (6.4 mmol) of resorcinol (Aldrich) and 1.1 mL of formalin solution (35 wt % formaldehyde, Aldrich) were added, and the reaction mixture was stirred at 30 °C for 22 h. It was then heated for 24 h at 100 °C under static conditions in a Teflon autoclave. The solid product was recovered by centrifugation and dried at 100 °C. Finally, the polymeric microspheres were carbonized under N_2 at 800 °C (5 °C/min, 1 h).

N-Doped Carbon. A nitrogen-rich polymer (poly(benzoxazine-*co*-resol)) was used as precursor to synthesize the N-doped carbons. The synthesis procedure is similar to that recently reported by Hao et al.[36] In a typical synthesis, 0.42 g (0.033 mmol) of Pluronic F-127 (Aldrich) and 1 g (9.1 mmol) of resorcinol were dissolved in a mixture of water (3 mL) and ethanol (3.8 mL) under magnetic stirring at room temperature. Afterward, 0.25 mL (1.32 mmol) of tetraethylenepentamine (Aldrich) was injected into the above solution which was then stirred for 30 min at room temperature. Subsequently, 1.5 mL of formalin solution (18.5 mmol of formaldehyde) was added. The resulting reaction mixture was stirred for 10 min. The solution was then poured into a Teflon autoclave which was placed in an oven at 90 °C and left for 4 h. The resulting polymeric monolith was dried at 50 °C for 24 h and then carbonized under N_2 at 800 °C (5 °C/min, 1 h).

Physical Activation. In order to increase the porosity, the carbonized materials were activated by using CO_2 as gasifying agent. The reaction was carried out in a thermogravimetric system (CI Electronics), which allowed one to know the gasification rate to be followed all the time. In a typical gasification experiment, around 200 mg of carbonized material was employed. In order to ensure a uniform activation, the gasification rates were restricted to $\sim$1–2%·h^{-1}. The gasification rate was controlled by modifying the reaction temperatures at around 800 °C (±20 °C). By means of this gasification procedure, it was possible to fabricate porous carbons with well-defined activation degrees rising from 15% to 47%. The carbons thus produced were denoted as $C - x$ or $CN - x$ for undoped or N-doped carbons, respectively, where x was a number that referred to the gasification degree (see Table 1).

Characterization of Materials. The nitrogen sorption isotherms of the carbon samples were measured at −196 °C using a Micromeritics ASAP 2020 sorptometer, whereas the carbon dioxide isotherms were measured in the −15 to 25 °C range using a Micromeritics TriStar II sorptometer. The apparent surface area (S_{BET}) was calculated from the N_2 isotherms using the BET method. An appropriate relative pressure range was selected to ensure that a positive line intersect of multipoint BET fitting ($C > 0$) would be obtained and $V_{ads}(1 - p/p_o)$ would increase with p/p_o.[30,37] The total pore volume (V_p) was determined from the amount of nitrogen adsorbed at a relative pressure (p/p_o) of 0.99. The micropore volume (V_m^t) and micropore surface area (S_m^t) were obtained by applying a t-plot analysis (Harkins and Jura thickness equation) to the N_2 sorption isotherms. The micropore size distributions (MPSDs) were determined by means of the quenched-solid density functional theory (QSDFT) method applied to the nitrogen adsorption data and assuming a slit pore model.

The CO_2 adsorption data obtained at 0 °C were used to analyze the narrow microporosity by means of the Dubinin–Radushkevich (D–R) equation[38]

$$V = V_o \exp[-(A/\beta E_o)^2] \quad (1)$$

where V is the volume filled at a temperature T and the relative pressure (p/p_o), V_o is the micropore volume, $A = RT \ln (p_o/p)$, and E_o and β are the characteristic energy and the affinity coefficient ($\beta = 0.35$ for CO_2), respectively. The average micropore width, L, was calculated by means of the empirical correlation proposed by Stoeckli et al.:[39]

$$L\ (\text{nm}) = 10.8/(E_o - 11.4) \quad (2)$$

Scanning electron microscopy (SEM) images were obtained on a Quanta FEG650 (FEI) instrument. X-ray photoelectron spectroscopy (XPS) was carried out on a Specs spectrometer, using Mg Kα (1253.6 eV) radiation from a double anode at 150 w. Binding energies for the high resolution spectra were calibrated by setting C 1s to 284.6 eV. Elemental analysis (C, H, N) of the samples was carried out on a LECO CHN-932 microanalyzer.

ASSOCIATED CONTENT

Supporting Information

Particle size distributions of pristine and activated materials, comparison of the fraction of CO_2 adsorbed at different temperatures for pristine and activated materials, characteristic curves at different temperatures for N-free and N-doped materials, and XPS results. This material is available free of charge via the Internet at http://pubs.acs.org.

AUTHOR INFORMATION

Corresponding Author

*E-mail: martasev@incar.csic.es.

Notes

The authors declare no competing financial interest.

ACKNOWLEDGMENTS

The financial support for this research work provided by the Spanish MINECO (MAT2012-31651) is gratefully acknowledged. M.S. thanks the Spanish MINECO for the award of a Ramón y Cajal contract.

REFERENCES

(1) Presser, V.; McDonough, J.; Yeon, S. H.; Gogotsi, Y. *Energy Environ. Sci.* **2011**, *4*, 3059−3066.
(2) Sevilla, M.; Fuertes, A. B. *Energy Environ. Sci.* **2011**, *4*, 1765−1771.
(3) Xia, Y.; Mokaya, R.; Walker, G. S.; Zhu, Y. *Adv. Energy Mater.* **2011**, *1*, 678683.
(4) Siriwardane, R. V.; Shen, M.-S.; Fisher, E. P.; Losch, J. *Energy Fuel* **2005**, *19*, 1153−1159.
(5) Cavenati, S.; Grande, C. A.; Rodrigues, A. E. *J. Chem. Eng. Data* **2004**, *49*, 1095−1101.
(6) Simmons, J. M.; Wu, H.; Zhou, W.; Yildirim, T. *Energy Environ. Sci.* **2011**, *4*, 2177−2185.
(7) Bae, Y.-S.; Snurr, R. Q. *Angew. Chem., Int. Ed.* **2011**, *50*, 11586−11596.
(8) Dawson, R.; Stockel, E.; Holst, J. R.; Adams, D. J.; Cooper, A. I. *Energy Environ. Sci.* **2011**, *4*, 4239−4245.
(9) Lim, H.; Cha, M. C.; Chang, J. Y. *Macromol. Chem. Phys.* **2012**, *213*, 1385−1390.
(10) Wahby, A.; Ramos-Fernandez, J. M.; Martinez-Escandell, M.; Sepulveda-Escribano, A.; Silvestre-Albero, J.; Rodriguez-Reinoso, F. *ChemSusChem* **2010**, *3*, 974−978.
(11) Wei, H.; Deng, S.; Hu, B.; Chen, Z.; Wang, B.; Huang, J.; Yu, G. *ChemSusChem* **2012**, *5*, 2354−2360.
(12) Sevilla, M.; Falco, C.; Titirici, M. M.; Fuertes, A. B. *RSC Advances* **2012**, *2*, 12792−12797.
(13) Liu, R.; Wu, D.; Feng, X.; Müllen, K. *Angew. Chem., Int. Ed.* **2010**, *49*, 2565−2569.
(14) Sevilla, M.; Valle-Vigon, P.; Fuertes, A. B. *Adv. Funct. Mater.* **2011**, *21*, 2781−2787.
(15) Kim, K.-S.; Park, S.-J. *Electrochim. Acta* **2011**, *56*, 10130−10137.
(16) Horikawa, T.; Sakao, N.; Sekida, T.; Hayashi, J. i.; Do, D. D.; Katoh, M. *Carbon* **2012**, *50*, 1833−1842.
(17) Wang, D.-W.; Li, F.; Yin, L.-C.; Lu, X.; Chen, Z.-G.; Gentle, I. R.; Lu, G. Q.; Cheng, H.-M *Chem.—Eur. J.* **2012**, *18*, 5345−5351.
(18) Arstad, B.; Fjellva, H.; Kongshaug, K. O.; Swang, O.; Blom, R. *Adsorption* **2008**, *14*, 755−762.
(19) Bae, Y. S.; Snurr, R. Q. *Angew. Chem., Int. Ed.* **2011**, *50*, 11586−11596.
(20) Mello, M. R.; Phanon, D.; Silveira, G. Q.; Llewellyn, P. L.; Ronconi, C. M. *Microporous Mesoporous Mater.* **2011**, *143*, 174−179.
(21) Yue, M. B.; Chun, Y.; Cao, Y.; Dong, X.; Zhu, J. H. *Adv. Funct. Mater.* **2006**, *16*, 1717−1722.
(22) Hao, G.-P.; Li, W.-C.; Qian, D.; Lu, A.-H. *Adv. Mater.* **2010**, *22*, 853−857.
(23) Liu, L.; Deng, Q. F.; Ma, T. Y.; Lin, X. Z.; Hou, X. X.; Liu, Y. P.; Yuan, Z. Y. *J. Mater. Chem.* **2011**, *21*, 16001−16009.
(24) Plaza, M. G.; Rubiera, F.; Pis, J. J.; Pevida, C. *Appl. Surf. Sci.* **2010**, *256*, 6843−6849.
(25) Wang, L.; Yang, R. T. *J. Phys. Chem. C* **2012**, *116*, 1099−1106.
(26) Zhu, X.; Hillesheim, P. C.; Mahurin, S. M.; Wang, C.; Tian, C.; Brown, S.; Luo, H.; Veith, G. M.; Han, K. S.; Hagaman, E. W.; Liu, H.; Dai, S. *ChemSusChem* **2012**, *5*, 1912−1917.
(27) Dubinin, M. M. *Carbon* **1989**, *27*, 457−467.
(28) Gregg, S. J.; Sing, K. S. W. In *Adsorption, surface area and porosity*; Academic Press: London, 1991.
(29) Sing, K. S. W. In *Porosity in carbons: characterization and applications*; Patrick, J. W., Ed.; Edward Arnold: London, 1995; Ch. 2, p 49.
(30) Rouquerol, F.; Rouquerol, J.; Sing, K. In *Adsorption by powders and porous solids: principles, methodology and applications*; Academic Press: San Diego, 1999.
(31) Dubinin, M. M. In *Chemistry and Physics of carbon*; Walker, P.L., Jr., Ed.; Marcel Dekker: New York, 1966; Vol. 2, p 56.
(32) Everett, D. H.; Powl, J. C. *J. Chem. Soc., Faraday Trans.* **1976**, *72*, 619−636.
(33) Cazorla-Amorós, D.; Alcañiz-Monge, J.; Linares-Solano, A. *Langmuir* **1996**, *12*, 2820−2824.
(34) Dubinin, M. M. *J. Colloid Interface Sci.* **1967**, *23*, 487−499.
(35) Liu, J.; Qiao, S. Z.; Liu, H.; Chen, J.; Orpe, A.; Zhao, D.; Lu, G. Q. *Angew. Chem.* **2011**, *123*, 5894.
(36) Hao, G.-P.; Li, W.-C.; Qian, D.; Wang, G.-H.; Zhang, W.-P.; Zhang, T.; Wang, A.-Q.; Schuth, F.; Bongard, H.-J.; Lu, A.-H. *J. Am. Chem. Soc.* **2011**, *133*,, 11378−11388..
(37) ISO. *ISO standard 9277:2010, Determination of the specific surface area of solids by gas adsorption - BET method*, Second Edition of ISO 9277; ISO: Geneva, 2012.
(38) Dubinin, M. M. *Chem. Rev.* **1960**, *60*, 235−241.
(39) Stoeckli, H. F.; Rebstein, P.; Ballerini, L. *Carbon* **1990**, *28*, 907−909.